Journal of Quantitative Spectroscopy & Radiative Transfer 112 (2011) 310–319

Contents lists available at ScienceDirect

Journal of Quantitative Spectroscopy & Radiative Transfer

journal homepage: www.elsevier.com/locate/jqsrt

Dust aerosol forward scattering effects on ground-based aerosol optical depth retrievals

J.M. Ge [a,b,*], J. Su [a,b], Q. Fu [a,b], T.P. Ackerman [b], J.P. Huang [a]

[a] Key Laboratory for Semi-Arid Climate Change of the Ministry of Education and College of Atmospheric Sciences, Lanzhou University, Lanzhou 730000, PR China
[b] Department of Atmospheric Sciences, University of Washington, Seattle, WA 98105, USA

ARTICLE INFO

Keywords:
Forward scattering
Dust aerosol
Radiative transfer

ABSTRACT

Monte Carlo radiative transfer calculations are performed to examine the forward scattering effects on retrievals of dust aerosol optical depth (AOD) from ground-based instruments. We consider dust aerosols with different AOD, effective radius and imaginary refractive index at 0.5 μm wavelength. The shape of dust aerosols is assumed to be spheroids and the equivalent spheres that preserve both volume and projected area (V/P) are also considered. The single-scattering albedos and asymmetry factors of spheroids and V/P-equivalent spheres have small differences, but the scattering phase functions are very different for the scattering angle range ∼90–180°. The relative errors of retrieved AOD caused by forward scattering effects due to the differences between the single-scattering properties of spheroids and spheres are similar. It is shown that at solar zenith angle (SZA) smaller than ∼70° the effect of the forward scattering is generally small although the relative errors in retrieved AOD can be as large as −10% when r_e=2. However, the largest relative errors, which can reach −40%, appear at high SZA (>∼70°) with AOD larger than 1. This is not caused by the increase of forward scattering intensity, but is due to the strong attenuation of solar direct beam.

1. Introduction

Aerosols can directly affect climate system by scattering and absorbing the incoming solar radiation and indirectly by changing the microphysics of clouds [1]. A great number of works have been done to study aerosol optical properties [2–4]. The aerosol optical depth (AOD) is the most important quantity to estimate the impact of aerosols on radiative energy budget. The AOD can be retrieved from the observation of spectral solar radiation reaching at the surface or reflected at the top of the atmosphere. While satellite observations provide the global coverage of AOD, the ground-based observations are much more reliable and are often used to calibrate and validate the AOD retrievals from satellite [5]. The widely employed ground-based instruments for the AOD retrievals include the sun photometers such as CIMEL [6] and the multi-filter rotating shadow-band radiometer (MFRSR [7]). These instruments have a finite fields of view (FOV) angle, which receives not only the direct solar beam but also some diffuse light that is scattered into the forward direction. This may cause an overestimation of measured direct solar irradiance and thus underestimation of retrieved AOD. In order to obtain the true AOD, the forward scattering light into the instruments' FOV should be taken into account.

Dust, a major aerosol in the atmosphere, usually has large optical depth and particle size [8]. Thus, the forward-scattering effects may be significant for dust aerosols. In addition, the shapes of dust particles are exclusively non-spherical [9–11], which have a different scattering phase function from those of spheres [12]. In

* Corresponding author at: Key Laboratory for Semi-Arid Climate Change of the Ministry of Education and College of Atmospheric Sciences, Lanzhou University, Lanzhou 730000, PR China.
E-mail address: gejm@lzu.edu.cn (J.M. Ge).

0022-4073/$ - see front matter © 2010 Elsevier Ltd. All rights reserved.
doi:10.1016/j.jqsrt.2010.07.006

this paper, Monte Carlo radiative transfer calculations are performed to evaluate the forward-scattering effects on the retrieval of dust aerosol optical depth from ground-based instruments. We assume that the shape of aerosol particles is spheroid for simple approximation of the complicated shapes of real dust aerosols and we also consider the equivalent spheres that preserve both volume and projected area. In the calculations of the single-scattering properties of dust aerosols, a combination of the T-matrix method [13,14] and the improved geometric optics method (IGOM [11,15]) is used for spheroids and Mie code [16] for spheres. A wide range of AOD, mean effective radius and solar zenith angles (SZA) are considered.

2. Monte Carlo simulations

The Monte Carlo method is a flexible approach to simulate photon transport by randomly sampling the variables from defined probability distributions [17]. Here we briefly describe our Monte Carlo radiative transfer code. Two coordinates are used to track the photon position and determine the direction of photon propagation. The first one is the Cartesian coordinator (x,y,z) while the second is (θ,ϕ) where θ and ϕ are the zenith and azimuth angles, respectively. A photon is launched to enter the aerosol layer along the direction of solar direct beam. A random number (RN), which represents the probability of a photon travelling a free path length (f_p) without interactions with aerosol particles, is generated so that

$$RN = \exp(-f_p \beta_e), \tag{2.1}$$

where β_e is the volume extinction coefficient. We check whether the photon goes out of the dust aerosol layer. If the photon is still in the layer, another RN is generated. If this RN is greater than single-scattering albedo, photon will be absorbed, otherwise, photon will be scattered. The scattering angle Θ can be determined from the scattering phase function $P(\Theta)$. Since the scattering phase function is normalized, we have

$$\frac{1}{2}\int_0^{\pi} P(\boldsymbol{\Theta})\sin\boldsymbol{\Theta}\, d\boldsymbol{\Theta} = 1, \tag{2.2}$$

where Θ is the scattering angle. The third RN is generated to solve the scattering angle following the equation

$$RN = \frac{1}{2}\int_{\cos\ \boldsymbol{\Theta}}^{1} P(\cos\ \boldsymbol{\Theta})d\cos\ \boldsymbol{\Theta}. \tag{2.3}$$

Here we assume that the aerosol particles are randomly oriented so that the azimuth angle is uniformly distributed between 0 and 2π and thus the azimuth angle after scattering is solved by ϕ=$2\pi RN$, where the RN is the forth random number generated. The above processes are repeated until the photon either goes outside of the aerosol boundaries (reflected or transmitted) or is absorbed and then a new photon is launched.

3. Single-scattering properties

The single-scattering properties including the single-scattering albedo and scattering phase function are required when we estimate the forward scattering effects by using the Monte Carlo method. Following Yang et al. [11] and Fu et al. [18], we assume that the shapes of dust particles are spheroids with an aspect ratio of 1.7 (i.e. a/b, where a and b are the rotational-symmetry and equatorial semi-axes, respectively). The real part of refractive index is 1.53 at 0.5 μm [11,18,19]. Two imaginary parts of refractive index, 0.001i and 0.008i, are used in our study [18]. To compute the single-scattering properties of spheroid dust particles, a combination of the T-matrix [13,14] and IGOM methods, which is originally developed by Yang et al. [11] and Yang and Liou [15], is used. The T-matrix is employed for the size parameter smaller than 50. When the size parameter is greater than 50, the IGOM is applied. Here the size parameter is defined as $2\pi r_v/\lambda$, where r_v is the radius of the volume equivalent sphere and λ is the wavelength. The spheroidal particles are assumed to be randomly oriented in space with $a(b)$ ranging from 0.071(0.042) to 21.37(12.57) μm, corresponding to a r_v from 0.05 to 15 μm.

In application of radiative energy budget calculation and remote sensing, the Mie theory is widely used to approximate non-spherical particles. However, the scattering phase functions of spheroidal particles are quite different from those of equivalent spheres derived by the Mie theory [11,18]. Herein we also consider the phase functions of spheres to examine the difference of forward scattering effect from that assuming spheroids. To calculate spherical phase function, the individual spheroid particle is converted into sphere particles that have both equivalent projected area (P) and volume (V) of the spheroid. By letting $P = n\pi r_{vp}^2$ and $V = n(4/3)\pi r_{vp}^3$, where n is the adjusted number of spheres to preserve both P and V for a spheroid, we have r_{vp}=$3V/4P$ [20,21].

In order to obtain the bulk single-scattering properties of dust aerosols, the lognormal size distribution [19] is employed:

$$\frac{dN(r_v)}{dr_v} = \frac{N_0}{r_v \ln(10)\sigma\sqrt{2\pi}} \exp\left\{-\frac{[\log(r_v/r_{vm})]^2}{2\sigma^2}\right\}, \tag{3.1}$$

Table 1
Single-scattering albedo (ϖ) and asymmetry factor (g) for both spheroid and V/P-equivalent sphere dust aerosol at 0.5 μm wavelength.

r_e (μm)	m=1.53+0.001i		m=1.53+0.008i	
	ϖ	g	ϖ	g
Sphere				
0.25	0.992	0.659	0.942	0.670
0.50	0.987	0.677	0.917	0.696
1.00	0.977	0.696	0.869	0.726
2.00	0.957	0.734	0.794	0.779
Spheroid				
0.25	0.992	0.667	0.942	0.680
0.50	0.987	0.680	0.916	0.705
1.00	0.976	0.690	0.866	0.732
2.00	0.954	0.716	0.788	0.781

where r_{vm} and σ are the mode radius and standard deviation, respectively, N_0 is the number density of dust aerosols and σ is assumed to be 0.4. We can then calculate the effective radius (r_e), bulk single-scattering albedo (ϖ) and phase function (P_{11}) according to the following formulas:

$$r_e = \frac{\int_{r_{v,\max}}^{r_{v,\max}} n r_{vp}^3 N(r_v)\,dr_v}{\int_{r_{v,\min}}^{r_{v,\max}} n r_{vp}^2 N(r_v)\,dr_v} = \frac{3}{4}\frac{\int_{r_{v,\min}}^{r_{v,\max}} VN(r_v)\,dr_v}{\int_{r_{v,\min}}^{r_{v,\max}} PN(r_v)\,dr_v}, \tag{3.2}$$

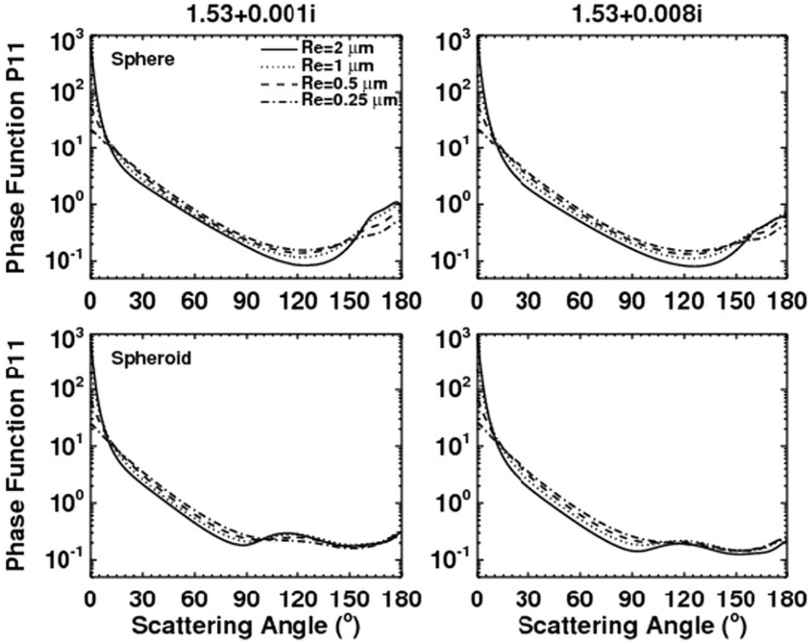

Fig. 1. Dust aerosol scattering phase functions for spheroids (lower panel) and *V*/*P*-equivalent spheres (upper panel) with two refractive indices and four effective radii at the wavelength of 0.5 μm.

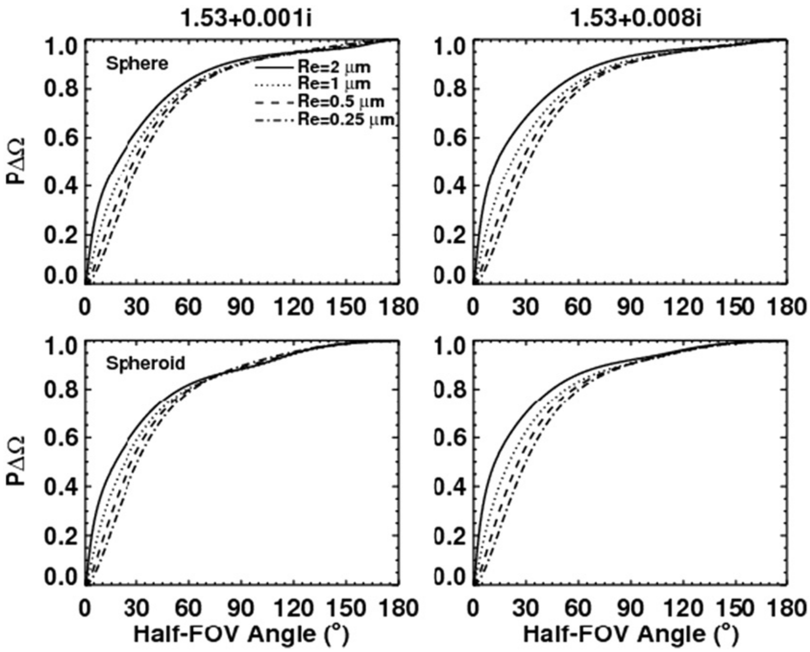

Fig. 2. $P\Delta\Omega$ as a function of half-FOV angles for spheroids and *V*/*P*-equivalent spheres with two refractive indices and four effective radii.

Table 2
The ratio of light singly scattered into instruments' FOV (i.e. $P\Delta\Omega$) at 0.5 μm wavelength.

r_e (μm)	m=1.53+0.001i		m=1.53+0.008i	
	CIMEL (%)	MFRSR (%)	CIMEL (%)	MFRSR (%)
Sphere				
0.25	0.06	0.43	0.06	0.45
0.50	0.14	0.99	0.15	1.06
1.00	0.45	2.72	0.51	3.05
2.00	1.54	7.62	1.86	9.17
Spheroid				
0.25	0.07	0.49	0.07	0.50
0.50	0.17	1.12	0.18	1.20
1.00	0.51	3.00	0.57	3.37
2.00	1.70	8.15	2.05	9.83

$$\varpi = \frac{\int_{r_{v,\min}}^{r_{v,\max}} Q_s PN(r_v)\,dr_v}{\int_{r_{v,\max}}^{r_{v,\max}} Q_e PN(r_v)\,dr_v}, \tag{3.3}$$

$$P_{11} = \frac{\int_{r_{v,\max}}^{r_{v,\max}} P'_{11} Q_s PN(r_v)\,dr_v}{\int_{r_{v,\min}}^{r_{v,\max}} Q_s PN(r_v)\,dr_v}, \tag{3.4}$$

where Q_s, Q_e and P'_{11} are the extinction and scattering efficiencies and scattering phase function, respectively, for individual particles.

4. Single forward scattering effects

When the AOD is small enough, the multiple-scattering processes are negligible. Following Russell et al. [22], the ratio of light scattered forward into the instruments'

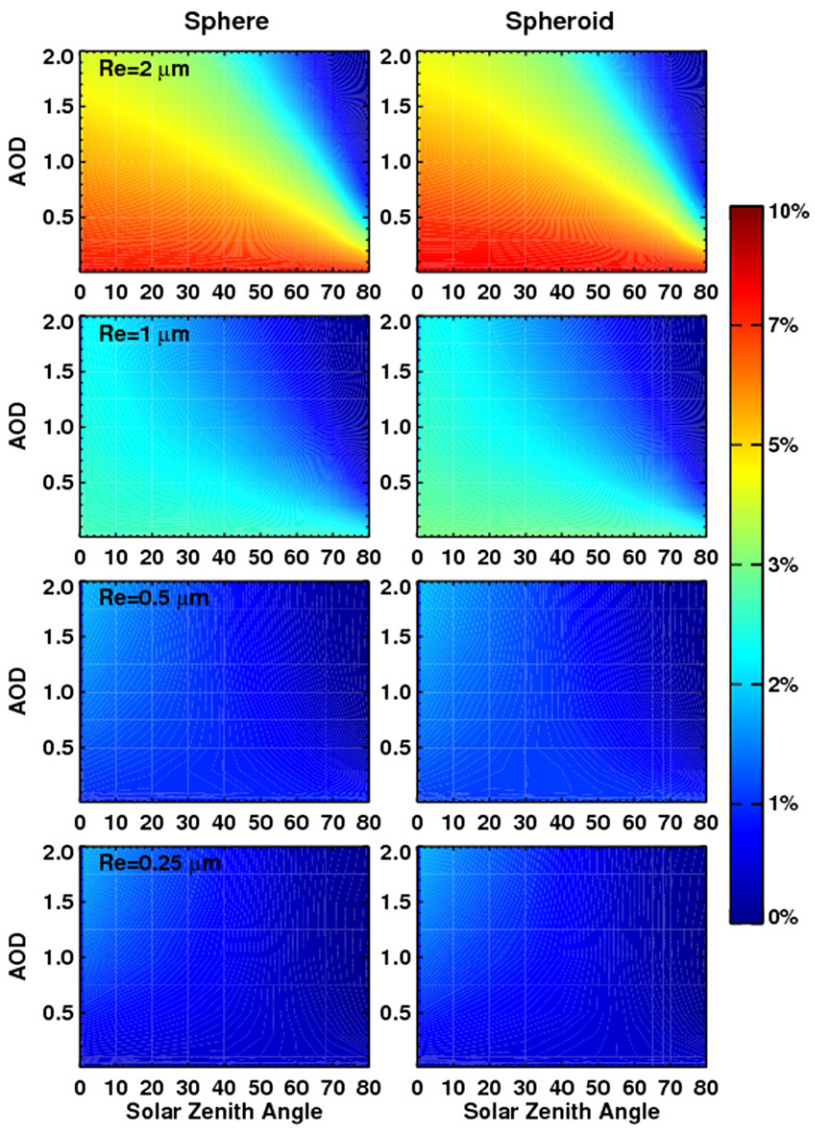

Fig. 3. The ratio of forward scattered light into the MFRSR's FOV to all scattered light versus optical depth and solar zenith angle with the refractive index of 1.53+0.001i and four effective radii of 2, 1, 0.5 and 0.25 μm from top to bottom at the wavelength of 0.5 μm. The left panel is for spheres and right panel is for spheroids.

FOV to the total scattered light can be estimated from the single-scattering process in the form

$$P\Delta\Omega = \int_0^{\eta_0} P_{11}(\Theta)\sin\Theta\, d\Theta \Big/ \int_0^{\pi} P_{11}(\Theta)\sin\Theta\, d\Theta = \frac{1}{2}\int_0^{\eta_0} P_{11}(\Theta)\sin\Theta\, d\Theta, \tag{4.1}$$

where η_0 is the half-FOV angle. Note the $P_{11}(\Theta)$ can be expanded in terms of Legendre polynomials P_l in the form

$$P_{11}(\cos\Theta) = \sum_{l=0}^{N} \varpi_l P_l(\cos\Theta), \tag{4.2}$$

where the moment ϖ_l is derived from the orthogonal properties of Legendre polynomials as follows:

$$\varpi_l = \frac{2l+1}{2}\int_{-1}^{1} P_{11}(\cos\Theta)P_l(\cos\Theta)d\cos\Theta. \tag{4.3}$$

Substituting Eq. (4.2) into Eq. (4.1) and considering the properties of Legendre polynomials, Eq. (4.1) can be further written as

$$P\Delta\Omega = \frac{1}{2}\left\{(1-\cos\eta_0) + \sum_{l=1}^{N}\frac{\varpi_l[P_{l-1}(\cos\eta_0)-P_{l+1}(\cos\eta_0)]}{2l+1}\right\}. \tag{4.4}$$

Here, ϖ_0=1 and $\varpi_1/3=g$ and g is the asymmetry factor. N is the number of expansion terms. Fu et al. [18] shows that the expansion with N=255 can converge to the exact scattering phase function for both spheres and spheroids, so we let N=255. Shiobara and Asano [23] used the $P\Delta\Omega$ and single-scattering albedo to calculate forward scattering correction factor. For given scattering phase function $P_{11}(\Theta)$ and half-FOV angle η_0, the single forward scattering portion $P\Delta\Omega$ can be easily estimated from Eq. (4.4). In Section 5, we will present the values of $P\Delta\Omega$ as a function

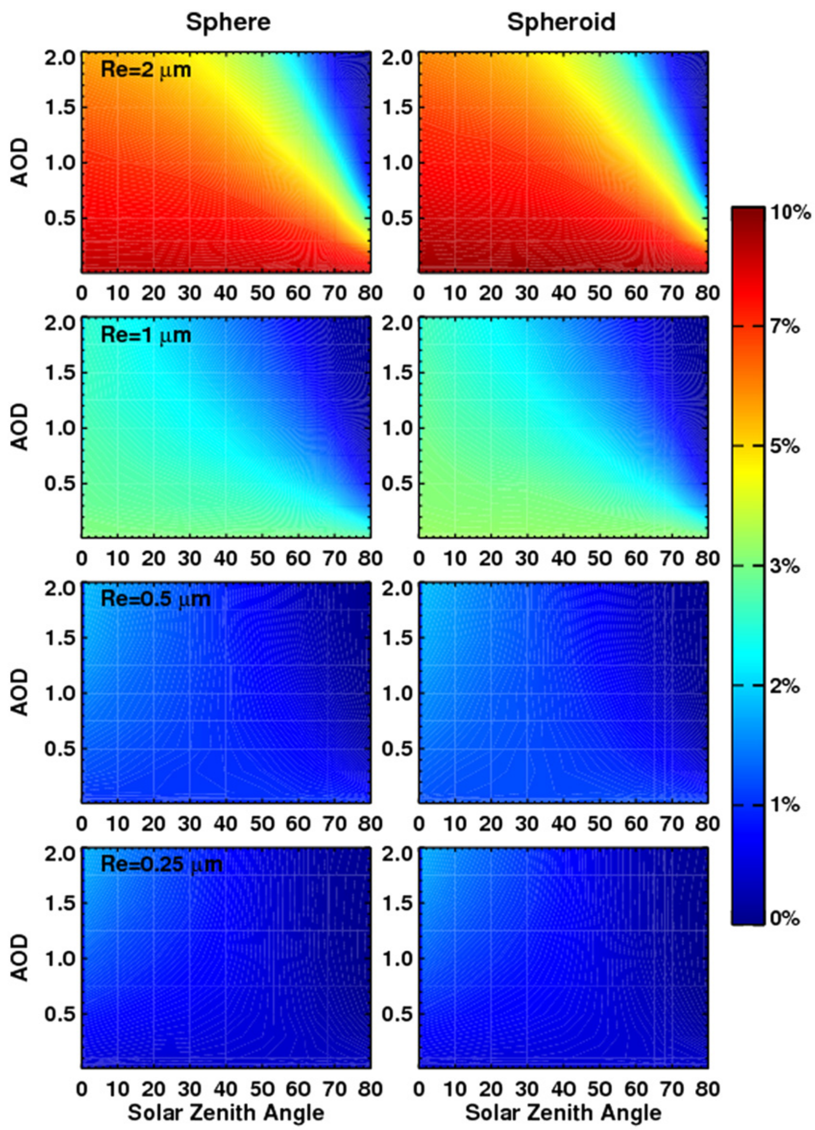

Fig. 4. Same as Fig. 3, but for the refractive index of 1.53+0.008i.

of η_0 and its dependence on effective radius, aerosol shape and refractive indices.

5. Results and discussions

Table 1 shows the single-scattering albedos and asymmetry factors of dust aerosol for both V/P-equivalent spheres and spheroids at 0.5 μm wavelength. Two imaginary refractive indices and four effective radii are considered for comparison. The ϖ and g vary with both effective radius and imaginary refractive index. Taking spheroids as an example, the value of ϖ decreases from 0.992 to 0.954 while g increases from 0.667 to 0.716 as r_e increases from 0.25 to 2 μm with a refractive index of 1.53+0.001i. For the imaginary part of 0.008i, the values of ϖ are smaller than that of 1.53+0.001i and range from 0.942 to 0.788. g varies from 0.68 to 0.781. We note that the difference of single-scattering albedos between spheroids and spheres is small (less than 0.06).

Fig. 1 shows the scattering phase functions of both spheroids and V/P-equivalent spheres, which are employed in the Monte Carlo simulations. We can see that the forward peaks of both spheroids and spheres sharply increase with the increase of r_e because larger particles have stronger forward scattering. The magnitudes of the scattering phase functions at forward peaks for spheroids and spheres are similar while the obvious differences appear at the back scattering directions (i.e. $>90^\circ$). From 90° to 140°, the spherical phase functions are smaller than that of spheroids but larger from 140° to 180°.

Fig. 2 is the ratio of the forward single-scattering light (i.e. $P\Delta\Omega$) from Eq. (4.4). The value of $P\Delta\Omega$ increases with increase in FOV angle and effective radius. When the FOV

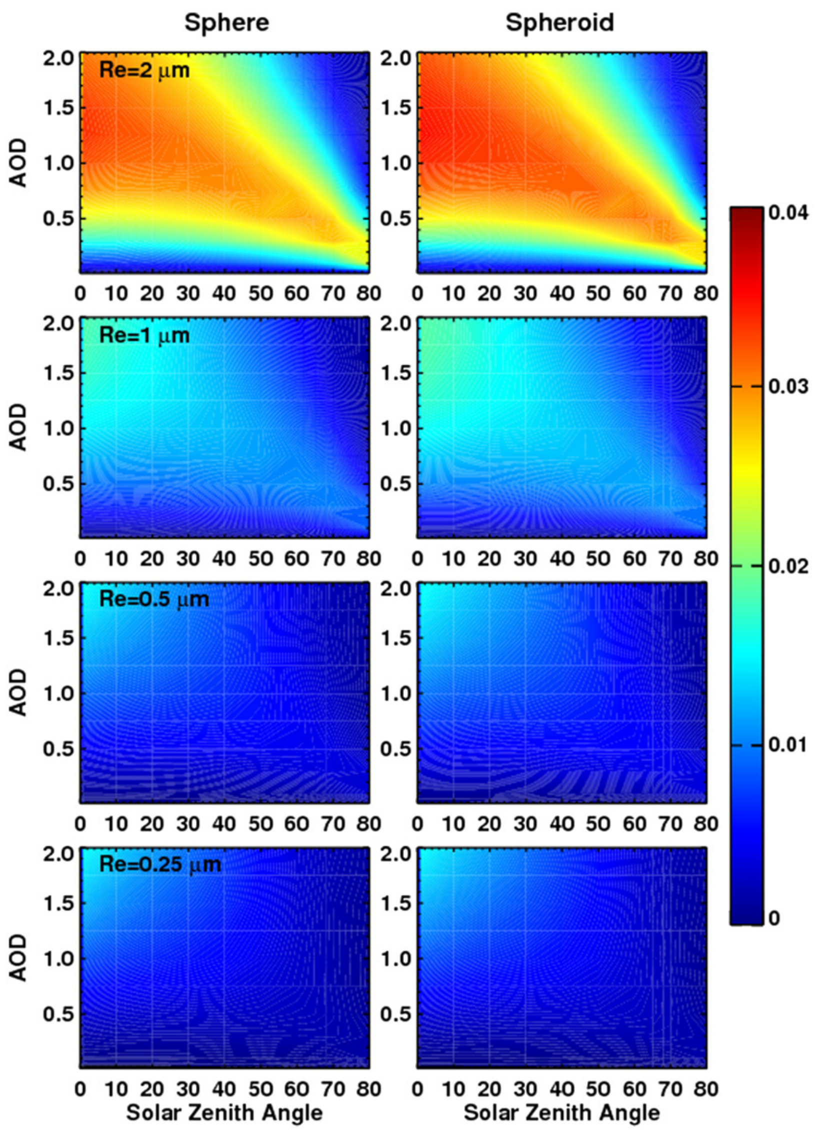

Fig. 5. The transmittance of forward scattered light versus optical depth and solar zenith angle with the refractive index of 1.53+0.001i and four effective radii of 2, 1, 0.5 and 0.25 μm from top to bottom at the wavelength of 0.5 μm. The left panel is for spheres and right panel is for spheroids.

angle is 360° (i.e. η_0=180), which means that the instrument can receive the scattered light in all directions, the value of $P\Delta\Omega$ becomes 1. Here we focus on ground-based instruments with specific FOV angles. The CIMEL that is the standard instrument of Aerosol Robotic Network (AERONET) has a narrow FOV angle of 1.2° [24] while the MFRSR has a FOV of ~3.3° [25]. Table 2 shows $P\Delta\Omega$ values for CIMEL and MFRSR. The $P\Delta\Omega$ values for the CIMEL are all smaller than 2.05%, indicating that the dust aerosol forward scattering may not significantly affect the accuracy of CIMEL retrieved AOD. However, for the MFRSR, the values of $P\Delta\Omega$ rapidly increase with effective radii. Almost 10% of the scattered light can be received by the MFRSR when the r_e is 2 μm and the imaginary refractive index is 0.008i. We also note that $P\Delta\Omega$ is insensitive to the dust aerosol shapes although the $P\Delta\Omega$ of spheroids is slightly larger than that of spheres.

To evaluate the forward scattering effects by considering the multiple-scattering processes with different AOD and solar zenith angles, we perform the Monte Carlo simulations of the photon transport through the dust aerosol layer. Fig. 3 shows the fraction of forward scattered light into the MFRSR's FOV to the total scattered light versus optical depth and solar zenith angle for the refractive index of 1.53+0.001i at 0.5 μm wavelength. The left panel shows the results by using spherical phase functions along with four effective radii of 2, 1, 0.5 and 0.25 μm while the right panel shows the results of spheroids. We can see that when the value of AOD is small (i.e. AOD=0.01) and thus the multiple scattering is less important, the forward scattering ratios are almost the same as those listed in Table 2. In Fig. 3, it also shows that the values of forward scattering ratio decrease with the increases of both AOD and solar zenith angle. However,

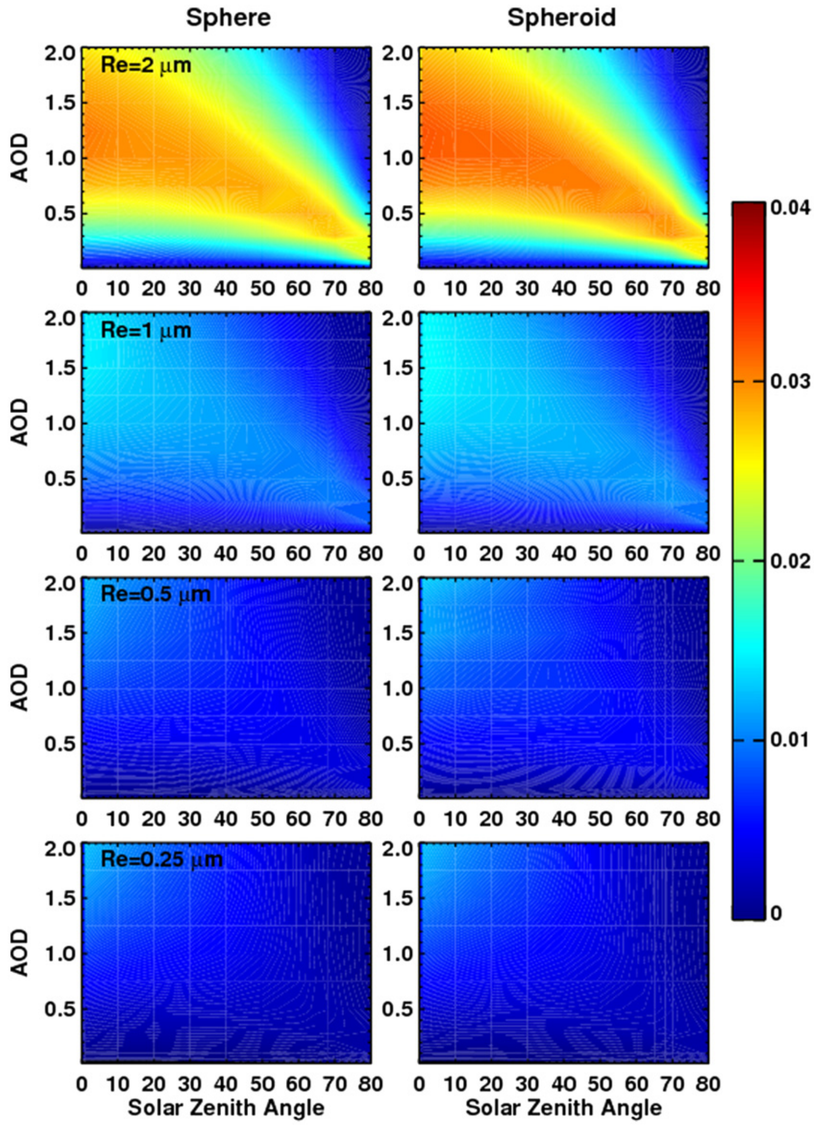

Fig. 6. Same as Fig. 5, but for the refractive index of 1.53+0.008i.

we found that the maximum value, for a given AOD, appears at the solar zenith angle of $\sim 1^\circ$ rather than 0°. For $r_e \le 0.5$ μm, less than 2% of all scattered light can be blocked as direct beam by MFRSR's shadowband and thus the forward scattering of dust aerosol may be not a serious problem. For $r_e \ge 1$ μm, the forward scattering gradually becomes important and it can amount to 10% of total scattered light when $r_e = 2$ μm for a AOD of 0.01. Fig. 4 is the same as Fig. 3 but for the refractive index of $1.53+0.008i$. The values of forward scattering ratio in Fig. 4 are relatively larger than those in Fig. 3. Here, we should point out that the ratio represents the relative strength of forward scattering. Although the forward scattering ratio decreases with increase in AOD and SZA, it does not mean that more light is forward scattered into the FOV at lower AOD and SZA. This is because aerosol does scatter more light when AOD is large or SZA is high. So the intensity of 10% forward scattering of total scattered light by the dust aerosol with optical depth of 0.01 at the SZA of 10° may be weaker than that of 5% forward scattered light by the aerosol with an optical depth of 2 at 70°.

To understand the absolute strength of forward scattering, we define the forward scattering transmittance, which is a ratio of the transmitted forward scattering intensity to the incident intensity. Here, the transmitted forward scattering intensity can be represented by the number of photons, which are mistakenly identified as direct beam by the MFRSR. The incident intensity is represented by the total number of lunched photons. Generally, forty thousand photons are enough to precisely simulate flux density; however, in our study we are interested in the intensity at a specific forward angle

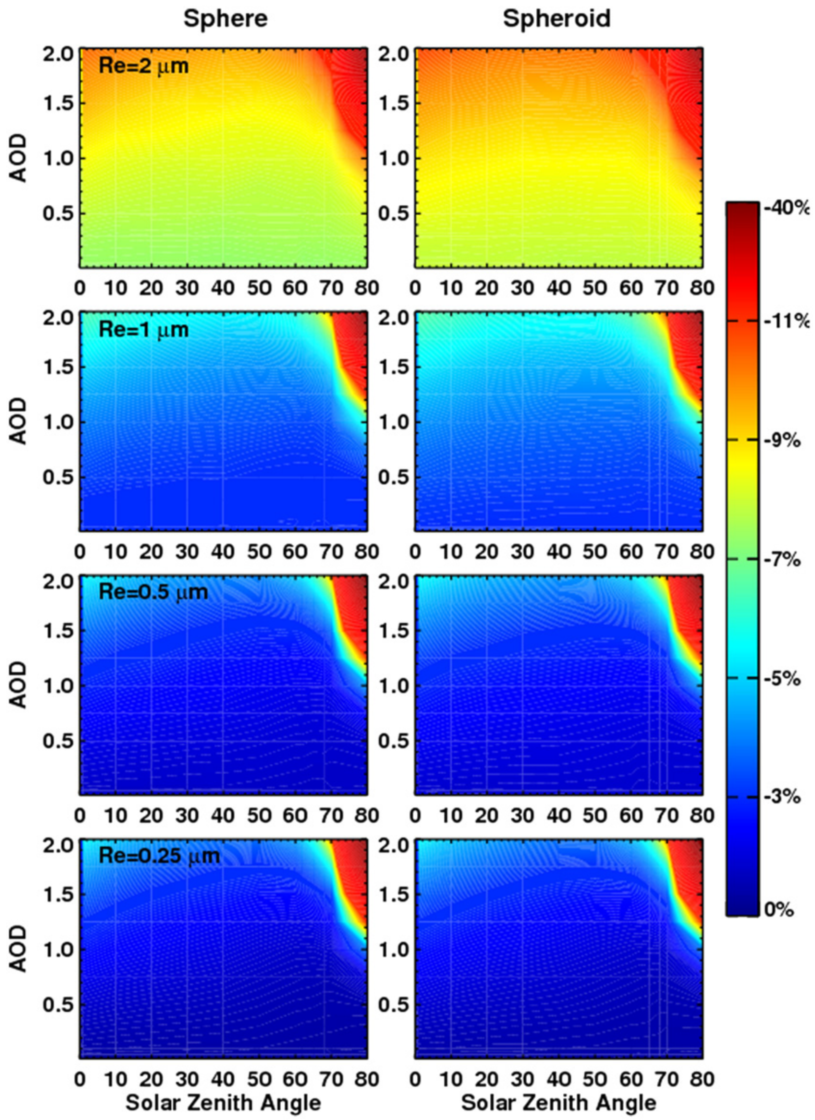

Fig. 7. The relative differences between apparent AOD and true AOD versus optical depth and solar zenith angle with the refractive index of $1.53+0.001i$ and four effective radii of 2, 1, 0.5 and 0.25 μm from top to bottom at the wavelength of 0.5 μm. The left panel is for spheres and right panel is for spheroids.

(i.e. half-FOV angle). To that end, a large number of photons (we use 1.5 million photons) are needed to get significant results in statistics. Fig. 5 is the same as Fig. 3 except for plotting the forward scattering transmittance. It is clear that more light can be scattered into the FOV at low solar zenith angle when AOD is larger than 0.5. When AOD is smaller than 0.5, the transmittance gradually increases as the solar zenith angle increases to 80°. Here we did not consider high solar zenith angle ($>80^\circ$), for which the AOD retrieval becomes unreliable because of large atmospheric refraction. Fig. 6 is the same as Fig. 5 but for the imaginary refractive index of 1.53+0.008*i*. We can see that in Fig. 6, the forward scattering transmittances are smaller than those in Fig. 5 due to the larger aerosol absorption.

From the Beer's Law, the AOD can be expressed as $\tau=\mu_0 \ln(I_0/I_s)$, where I_0 is the incident intensity at the top of atmosphere (TOA), I_s is the intensity received by ground instrument and μ_0 is the cosine of the solar zenith angle. For the apparent AOD, for which the forward scattering contribution has not been removed, I_s consists of two parts, i.e. the direct beam I_{dir} and the scattered light I_{dif}, which is wrongly blocked being direct beam by MFRSR. Thus the apparent AOD is smaller than true AOD. Figs. 7 and 8 show the relative error between the apparent AOD and true AOD from the Monte Carlo simulations. Generally, the error becomes smaller with the decrease of AOD and effective radius. The errors of spheroids (right panel) are slightly bigger than that of spheres (left panel). There are two areas where the errors are relatively larger. One appears at low solar zenith angle ($<\sim 20^\circ$) and the other occurs at high ($>\sim 60^\circ$) solar zenith angle with AOD greater than 1. The former is caused by strong forward scattering effect but the latter is clearly not caused by the same reason. Because,

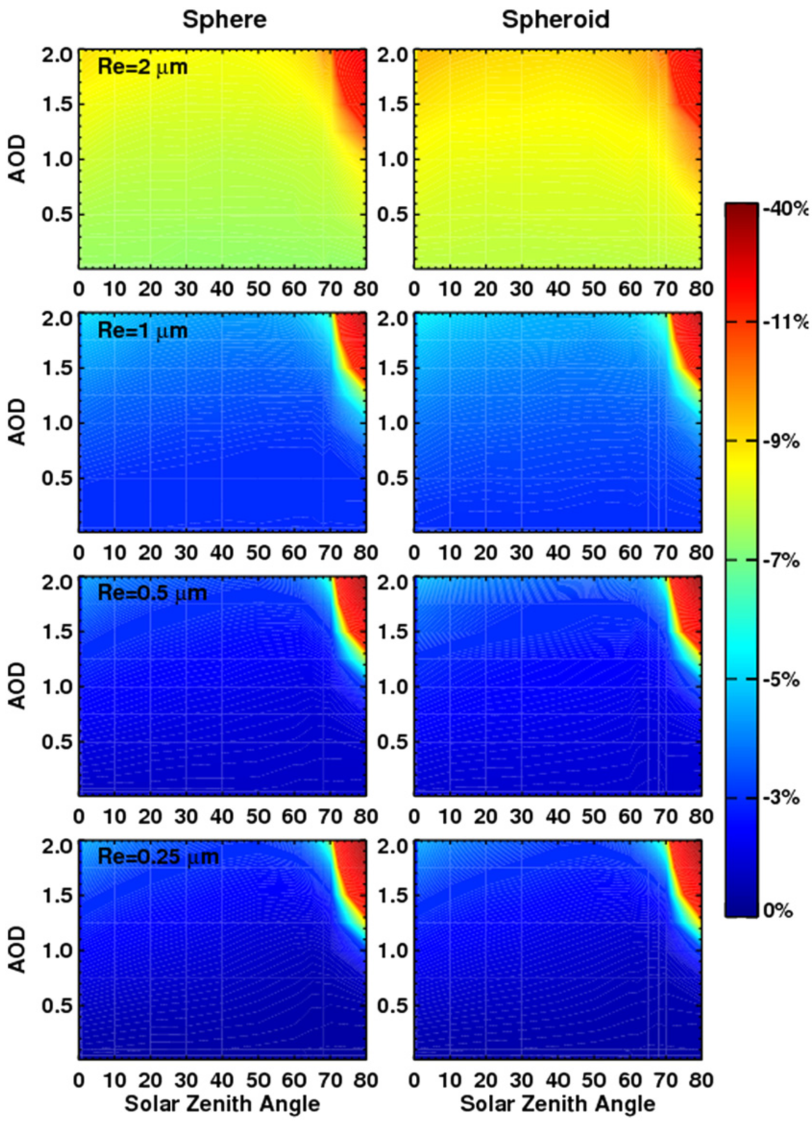

Fig. 8. Same as Fig. 7, but for the refractive index of 1.53+0.008*i*.

from Figs. 5 and 6, we know that the forward scattering intensity is much small at high SZA. The large errors, whose absolute values are greater than 11% at high SZA ($>70^{\circ}$) with large AOD (>1), are due to too much attenuation of direct light (i.e. I_{dir}) after passing through a thick optical path. Thus, under these circumstances, the apparent AOD must be corrected to get the true AOD. When effective radius is less than 1 μm and AOD is less than 1, the relative errors between the apparent AOD and true AOD are smaller than -3%. Forward scattering effects can be negligible under this situation.

6. Conclusion

The forward scattering effects on retrieval of dust aerosol optical depth from the MFRSR are analyzed at 0.5 μm for two refractive indices and four effective radii. The single-scattering albedos and scattering phase functions of both spheroids and V/P-equivalent spheres are considered. For the single-scattering albedos, the differences between spheres and spheroids are small while the differences in the scattering phase functions are significant. Since the $P\Delta\Omega$ is usually parameterized to correct apparent AOD, we examine this parameter first. For the CIMEL, the values of $P\Delta\Omega$ are all smaller than 2.05% because of the very narrow FOV angle. For the MFRSR's FOV, the $P\Delta\Omega$ varies from 0.43% to 9.83% depending on r_e and the refractive indices.

The Monte Carlo simulation of photon transport is used to estimate forward scattering effects on the MFRSR AOD retrievals by considering multiple-scattering processes. The intensity of forward scattered light into the MFRSR's FOV gradually increases with the SZAs when the value of AOD is less than 0.5. However, when the value of AOD is larger than 0.5, more light can be forward scattered into the FOV at lower SZAs. The relative errors between apparent AOD and true AOD increase with both effective radius and AOD. When the effective radius and AOD are less than 1, the errors are smaller than -3%. The relatively larger errors occur at the SZA lower than 20° and higher than 60° with AOD larger than 1. The former is caused by strong forward scattering effect while the latter is due to the strong attenuation of direct solar beam.

Acknowledgements

This research is supported by the National Science Foundation of China under grants 40725015, 40633017 and 40975012 and the Fundamental Research Funds for the Central University (lzujbky-2009-157). QF is in part supported by DOE Grant DE-FG02-09ER64769. We thank Prof. P. Yang for providing the IGOM program.

References

[1] Ramanathan V, Crutzen PJ, Kiehl JL, Rosenfeld D. Aerosols, climate, and the hydrological cycle. Science 2001;294:2119–24.
[2] Osborne SR, Johnson BT, Haywood JM, Baran AJ, Harrison MAJ, McConnell CL. Physical and optical properties of mineral dust aerosol during the dust and biomass-burning experiment. J Geophys Res 2008;113:D00C03.
[3] McFarlane SA, Kassianov EI, Barnard J, Flynn C, Ackerman TP. Surface shortwave aerosol radiative forcing during the Atmospheric Radiation Measurement Mobile Facility deployment in Niamey, Niger. J Geophys Res 2009;114:D00E06.
[4] Ge JM, Su J, Ackerman TP, Fu Q, Huang JP, Shi JS. Dust aerosol optical properties retrieval and radiative forcing over northwestern China during the 2008 China–US joint field experiment. J Geophys Res 2010;115:D00K12, doi:10.1029/2009JD013263.
[5] Dubovik O, Smirnov A, Holben BN, King MD, Kaufman YJ, Eck TF, et al. Accuracy assessments of aerosol optical properties retrieved from Aerosol Robotic Network (AERONET) Sun and sky radiance measurements. J Geophys Res 2000;105(18):9791–806.
[6] Holben BN, Eck TF, Slutsker I, Tanré D, Buis JP, Setzer KA, et al. AERONET—a federated instrument network and data archive for aerosol characterization. Remote Sens Environ 1998;66:1–16.
[7] Harrison L, Michalsky J, Berndt J. Automated multifilter rotating shadow-band radiometer: an instrument for optical depth and radiation measurements. Appl Opt 1994;33(22):5118–25.
[8] Kim DH, Sohn BJ, Nakajima T, Takamura T, Takemura T, Choi BC, et al. Aerosol optical properties over East Asia determined from ground-based sky radiation measurements. J Geophys Res 2004; 109:D02209.
[9] Okada K, Heintzenberg J, Kai K, Qin Y. Shape of atmospheric mineral particles collected in three Chinese arid-regions. Geophys Res Lett 2001;28(16):3123–6.
[10] Gao Y, Anderson JR. Characteristics of Chinese aerosols determined by individual particle analysis. J Geophys Res Atmos 2001;106(18): 037–045.
[11] Yang P, Feng Q, Hong G, Kattawar GW, Wiscombe WJ, Mishchenko MI, et al. Modeling of the scattering and radiative properties of nonspherical dust-like aerosols. J Aerosol Sci 2007;38:995–1014.
[12] Mishchenko MI, Travis LD, Kahn RA, West RA. Modeling phase functions for dustlike tropospheric aerosols using a shape mixture of randomly oriented polydisperse spheroids. J Geophys Res 1997;102:16831–47.
[13] Waterman PC. Matrix formulation of electromagnetic scattering. Proc IEEE 1965;53:805–12.
[14] Mishchenko MI, Travis LD. Light scattering by polydispersions of randomly oriented spheroids with sizes comparable to wavelengths of observations. Appl Opt 1994;33:7206–25.
[15] Yang P, Liou KN. Geometric-optics-integral-equation method for light scattering by nonspherical ice crystals. Appl Opti 1996;35: 6568–6584.
[16] Wiscombe WJ. Improved Mie scattering algorithms. Appl Opt 1980;19(9):1505–9.
[17] Liou KN. An introduction to atmospheric radiation [second version]. New York: Academic Press; 2002.
[18] Fu Q, Thorsen TJ, Su J, Ge JM, Huang JP. Test of Mie-based single-scattering properties of non-spherical dust aerosols in radiative flux calculations. J Quan Spectro Radiat Trsnsfer 2009; 110:1640–53.
[19] Levoni C, Cervino M, Guzzi R, Torricella F. Atmospheric aerosol optical properties: a database of radiative characteristics for different components and classes. Appl Opt 1997;36:8031–41.
[20] Fu Q, Sun WB, Yang P. Modeling of scattering and absorption by nonspherical cirrus ice particles at thermal infrared wavelengths. J Atmos Sci 1999;56:2937–47.
[21] Grenfell Tomas C, Stephen G Warren. Representation of a nonspherical ice particle by a collection of independent spheres from scattering and absorption of radiation. J Geophys Res 1999; 104(D24):31,697–709.
[22] Russell PB, Livingston JM, Dubovik O, Ramirez SA, Wang J, Redemann J, et al. Sunlight transmission through desert dust and marine aerosols: diffuse light corrections to Sun photometry and pyrheliometry. J Geophys Res 2004;109:D08207, doi:10.1029/2003JD004292.
[23] Shiobara M, Asano S. Estimation of cirrus optical thickness from Sun photometer measurements. J Appl Meteorol 1994;33:672–81.
[24] Holben BN, et al. An emerging ground-based aerosol climatology: aerosol optical depth from AERONET. J Geophys Res 2001;106: 12067–97.
[25] Kassianov EI, Flynn CJ, Ackerman TP, Barnard JC. Aerosol single-scattering albedo and asymmetry parameter from MFRSR observations during the ARM Aerosol IOP 2003. Atmos Chem Phys 2007;7:3341–51.